energies

MDPI

Article

Quantitative Analysis of Amorphous Silica and Its Influence on Reservoir Properties: A Case Study on the Shale Strata of the Lucaogou Formation in the Jimsar Depression, Junggar Basin, China

Ke Sun [1,*], Qinghua Chen [1], Guohui Chen [2,3], Yin Liu [1] and Changchao Chen [4]

1 School of Geosciences, China University of Petroleum (East China), Qingdao 266580, China; chenqhua@upc.edu.cn (Q.C.); liuyin@upc.edu.cn (Y.L.)
2 School of Earth Resources, China University of Geosciences, Wuhan 430074, China; chenguohui@cug.edu.cn
3 Key Laboratory of Theory and Technology of Petroleum Exploration and Development in Hubei Province, China University of Geosciences, Wuhan 430074, China
4 Exploration and Development Research Institite, PetroChina Tarim Oilfield Company, Korla 841000, China; ccccup1989@sina.com
* Correspondence: sunke@s.upc.edu.cn; Tel.: +86-185-6065-3166

Received: 30 October 2020; Accepted: 23 November 2020; Published: 24 November 2020

Abstract: To establish a new quantitative analysis method for amorphous silica content and understand its effect on reservoir properties, the amorphous silica (SiO_2) in the shale strata of the Lucaogou Formation in the Jimsar Depression was studied by scanning electron microscopy (SEM) observation, X-ray diffraction (XRD), and X-ray fluorescence spectrometry (XRF). Amorphous silica shows no specific morphology, sometimes exhibits the spherical or ellipsoid shapes, and usually disorderly mounds among other mineral grains. A new quantitative analysis method for observing amorphous SiO_2 was established by combining XRD and XRF. On this basis, while the higher content of amorphous SiO_2 lowers the porosity of the reservoir, the permeability shows no obvious changes. The higher the content of amorphous SiO_2, the lower the compressive strength and Young's modulus and the lower the oil saturation. Thus, amorphous SiO_2 can reduce the physical properties of reservoir rocks and increase the reservoir plasticity, which is not only conducive to the enrichment of shale oil but also increases the difficulty of fracturing in later reservoir development.

Keywords: amorphous SiO_2; X-ray diffraction; X-ray fluorescence spectrometry; scanning electron microscope; quantitative analysis; reservoir properties

1. Introduction

The success of shale gas exploration and development in North America has promoted the development of the shale gas industry around the world. At present, successful exploration and development of shale gas in China is mainly concentrated in the Sichuan Basin and surrounding areas, such as the Weiyuan, Zhaotong, Zhengan, and Jiaoshiba areas [1–3]. The shale sections containing commercial scale gas in these areas are located at the top of the Wufeng and the bottom of the Longmaxi Formations, corresponding to the 2-3 graphitic biozones of the Wufeng Formation and the 1-4 graphitic biozones of the Longmaxi Formation [4,5]. These high-quality shale sections contain high content of silica: as much as 60% [6–11]. Although there are different opinions about the evidence of biogenesis, most researchers consider that the silica in these high-quality shale sections has biogenic sources [12–17]. Shale oil sources are mainly concentrated in basins in China, where lacustrine shale is widely developed, such as the Ordos, Songliao, and Bohai Bay Basins. Shale oil

exploration has been particularly successful in the second member of the Kongdian Formation in Cangdong Depression of Bohai Bay Basin, where commercial-scale oil has been obtained in several wells [18]. This quartz-feldspathic shale exhibits good quality, high TOC content, and high hydrocarbon potential [18]. The tuffaceous shale sections of the Lucaogou Formation shale strata in the oil reservoir of the Malang Depression contain high total organic carbon and exhibit high hydrocarbon generation potential. These tuffaceous shales are also mainly composed of quartz and feldspar [19]. In both marine shale gas and or lacustrine shale oil reservoirs, silica is an important component, having a significant impact on shale reservoir properties, organic matter enrichment, shale oil and gas accumulation, and fracturing potential [14,15,20–25]. Hence, silica is a hot spot in shale reservoir research at present.

Studies on silica diagenesis have shown that the end members are amorphous SiO_2 and crystalline quartz. The quartz can be further divided into authigenic quartz formed during diagenesis and detrital quartz from deposition. During diagenesis, amorphous SiO_2 will gradually change from the amorphous state (opal-A) to the cryptocrystalline state and finally to the fully crystalline state (α-quartz), which is authigenic quartz. Amorphous SiO_2 can be from biological organisms or an abioticearly diagenesis stage. Some studies suggest that amorphous SiO_2 has already transformed into crystalline quartz during early diagenesis (Ro is 0.35%~0.5%) [23,24]. Others suggest that the conversion of amorphous SiO_2 to crystalline quartz in shale reservoirs may be much later, because amorphous SiO_2 has been seen in the middle diagenetic stage A (Ro is 0.5%~1.3%) [21]. During clay mineral conversion, a large amount of silica is generated, and its content is closely related to mineral composition, crystallinity, and thermal conditions; it also affects the physical properties and brittleness of the reservoir [26–28]. The influence of amorphous SiO_2 on reservoir properties can make a large difference in different evolution stages. From the beginning of diagenesis to the cryptocrystalline state, formation porosity has been shown to be reduced from about 45% to less than 25%, and the permeability declines to be difficult to be measured [29]. In the authigenic quartz stage, reservoir physical properties and brittleness increases instead, which improves reservoir fracturability [29]. Thus, it can be seen that amorphous SiO_2 also plays a great impact on reservoir properties. If the influence of amorphous SiO_2 on reservoirs can be clarified, it will be of great significance for evaluating shale oil reservoirs and fracturing potential, especially for immature lacustrine shale oil reservoirs.

Accurate calculation of amorphous SiO_2 content is the key problem to understand the influence of amorphous SiO_2 on reservoir properties. There are currently four methods for the quantitative analysis of amorphous SiO_2 in heterogeneous systems. The first is chemical dissolution, which means removing minerals other than amorphous SiO_2. However, chemical dissolution incudes crystalline, which affects the accuracy of quantitative analysis. The second is quantitative analysis using XRD as proposed by Lin (1997) [30]. Although the method is correct in theory, human error enters into in the quantification [31]. Thirdly, Chu (1998) proposed a new quantitative XRD method based on the increment method proposed by Popović et al. (1983) [32,33], but this method required preparation of a standard sample having a known mineral composition and proportions; the error was relatively large in the actual experiment. Fourth, Huang et al. (2015) established a calculation method for amorphous SiO_2 in the Yanchang Formation shale of the Ordos Basin by using XRD combined with QEMSCAN analysis [34]. However, this method has two disadvantages. Firstly, it is too expensive to conduct large-scale tests. Secondly, the mineral composition obtained by QEMSCAN analysis can be understood as a volume percentage. Hence, it needs to be converted into a mass percentage, but the density of minerals was not determined in Huang et al. (2015) [34].

In view of the shortcomings of previous methods for calculating the content of amorphous silica [30–34], a new quantitative analysis method for amorphous silica content was established in this research, based on XRD and XRF analysis of core samples from the Lucaogou Formation in the Jimsar Depression. Through the analysis of the relationship between physical parameters, rock mechanical parameters, oil saturation, and amorphous silica content in shale strata, the effect of amorphous SiO_2 on reservoir properties and its geological significance was determined.

2. Geological Settings

The Junggar Basin is located in the northwestern part of China with an area of about 1.30×10^5 km^2 (Figure 1A); it is geotectonically located at the intersection of Kazakhstan, Siberian, and Tarim plates. The Jimusar Depression is in the southeast of Junggar Basin, covering an area of 1.278×10^3 km^2; it is surrounded by the Shaqi Uplift to the north, the Guxi Uplift to the east, the Fukang faults zone to the south, and the Santai Uplift to the west (Figure 1B). The periphery of the Jimsar Depression is bounded by six faults (Figure 1B). The Permian Lusaogou Formation has a thickness of 200~350 m and is in conformable contact with the lower Jingjingzigou Formation and in unconformable contact with the upper Wutonggou Formation (Figure 1C). The Lucaogou Formation is mainly composed of deep and semideep lake facies formed of fine-grained, mixed sedimentary rocks [35,36]. It was formed in an intracontinental rifted saline lake basin environment, accompanied by volcanic eruptions and hydrothermal activity [37,38]. Since September 2011, J25, J23, J28, J30, and other exploration and evaluation wells have been successively drilled in the Jimusar Depression, oil testing shows industrial potential, and shale oil was discovered in the Lucaogou Formation. After nine years of development, the calculated reserves of shale reservoir have reached 11.12×10^8 t [39].

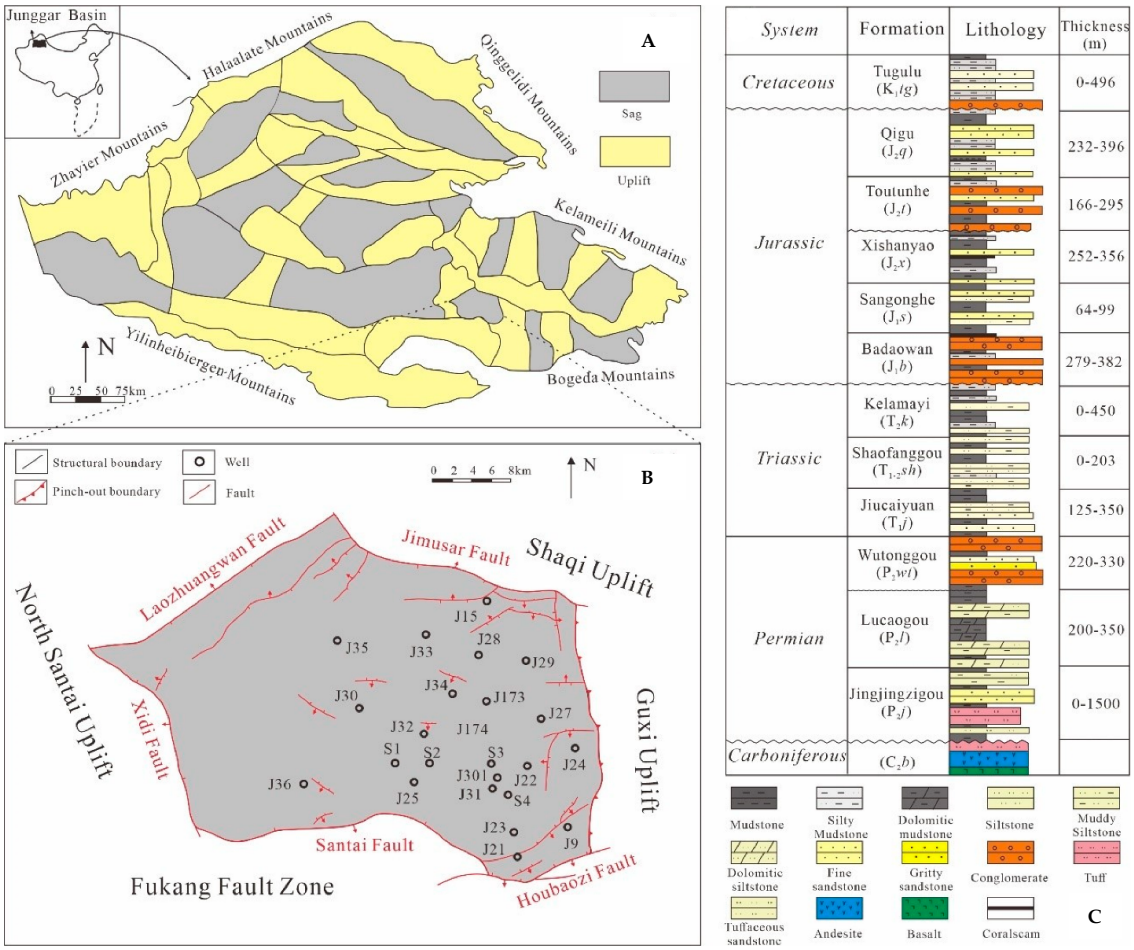

Figure 1. Diagrams showing (**A**) Junggar tectonic units and location of the Jimusar Depression, (**B**) structure and well location map of the Jimsar Depression, and (**C**) the stratigraphic sequence from Upper Caboniferous to Lower Cretaceous in the Jimsar Depression (modified from [40]).

3. Materials and Methods

3.1. Materials

The samples of the Lucaogou Formation in this study are from four cored wells (S1–S4) in the Jimsar Depression (Figure 1B). We selected 42 samples that met experimental needs. Their lithology includes tuffaceous shale (also called siliceous shale), shale, dolomite, and dolomitic mudstone. Generally, the lithology can be divided into three lithofacies: tuffaceous shale lithofacies, transitional lithofacies (also called mixed lithofacies), and carbonate lithofacies [41,42].

3.2. Experimental Method

XRD analysis was completed at Sichuan Keyuan Engineering Technology Testing Center. XRF analysis, rock mechanics experiments, and reservoir physical properties analysis were completed at the Experimental Research Center of East China Oil and Gas Branch of Sinopec.

3.2.1. XRD and XRF Analysis

The mineral composition of samples was obtained by XRD, which was determined on the premise of deducting background values through the Jade 5.0 software package. The principle of XRD analysis is that different minerals show different XRD diffraction effects. Data calculated by the XRD accurately represents the relative content of each mineral. However, XRD cannot measure the content of amorphous silica because it shows no diffraction peaks.

The secondary X-rays were emitted when the X-ray irradiated on the material. Different elements show their specific secondary X-ray with certain features or wavelength characteristics. XRF analysis uses secondary X-rays to convert the data into specific elements and their abundance. Elemental Si occurs in quartz, plagioclase, k-feldspar, clay minerals, and amorphous silica.

3.2.2. Rock Mechanics Experiment

Samples were tested using a TAW-2000 computer-controlled electrohydraulic servo testing machine under constant confining pressure conditions. The size of test samples is 25 mm (diameter) × 50 mm (length). In the process of testing, strain rate was controlled by the DUOLI microcomputer control system, mostly 0.01–0.03, which was convenient to obtain smooth stress–strain curves. The compressive strength, Young's modulus, and Poisson's ratio can be calculated by the stress–strain curves.

3.2.3. Reservoir Physical Properties

The total porosity was obtained by calculating the difference between the bulk density and the skeleton density. Permeability was obtained by calculating the expansion of He with increasing pressure (5 MPa–30 Mpa) at a constant temperature. Oil saturation was measured by nuclear magnetic resonance (NMR).

3.3. A New Method for Calculating the Content of Amorphous SiO_2

In this study, a new method for quantitative analysis of amorphous SiO_2 in the Lucaogou Formation of the Jimusar Depression was established by using a combination of XRD and XRF. Through XRD analysis, the shale strata mainly consist of quartz, plagioclase, potash feldspar, dolomite, calcite, pyrite, and clay minerals (Figure 2A). Elemental Si is in quartz, plagioclase, potash feldspar, and clay minerals.

The combination of XRD and XRF can calculate amorphous silica as follows. Suppose the sample mass is M, where the mass of amorphous SiO_2, quartz, plagioclase, K-feldspar, and clay minerals are respectively represented by m_{SiO_2}, m_{quartz}, $m_{plagioclase}$, $m_{K-feldspar}$, and m_{clay}.

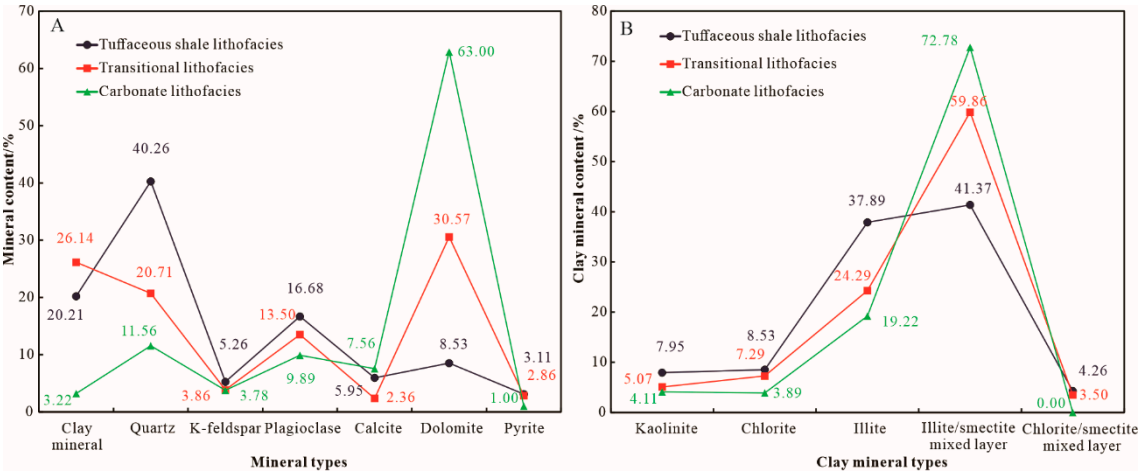

Figure 2. Mineral composition of different lithofacies samples in the Lucaogou Formation. (**A**) The mineral content of the different lithofacies; (**B**) clay mineral composition in the different lithofacies.

According to XRD analysis:

$$\frac{m_{quartz}}{M - m_{SiO_2}} = W_{quartz}. \tag{1}$$

$$\frac{m_{plagioclase}}{M - m_{SiO_2}} = W_{plagioclase} \tag{2}$$

$$\frac{m_{K-feldspar}}{M - m_{SiO_2}} = W_{K-feldspar} \tag{3}$$

$$\frac{m_{clay}}{M - m_{SiO_2}} = W_{clay} \tag{4}$$

The W_{quartz}, $W_{plagioclase}$, $W_{K-feldspar}$, and W_{clay} represent the percentage of quartz, plagioclase, *k*-feldspar, and clay minerals measured by XRD analysis.

According to XRF analysis:

$$\frac{m_{SiO_2} \times P_{Si-SiO_2} + m_{quartz} \times P_{Si-quartz} + m_{plagioclase} \times P_{Si-plagioclase}}{M} + \frac{m_{K-feldspar} \times P_{Si-K-feldspar} + m_{Clay} \times P_{Si-clay}}{M} = W_{\mathrm{Si}} \tag{5}$$

The mass percentages of Si in amorphous SiO_2, quartz, plagioclase, k-feldspar, clay minerals, and the sample are represented by P_{Si-SiO_2}, $P_{Si-quartz}$, $P_{Si-plagioclase}$, $P_{Si-K-feldspar}$, $P_{Si-clay}$, and W_{Si}, respectively.

Placing Formulas (1)–(4) into Formula (5), thus creating Formula (6)

$$\frac{m_{SiO_2} \times P_{Si-SiO_2} + W_{quartz} \times (M - m_{SiO_2}) \times P_{Si-quartz} + W_{plagioclase} \times (M - m_{SiO_2}) \times P_{Si-plagioclase}}{M} + \frac{W_{K-feldspar} \times (M - m_{SiO_2}) \times P_{Si-K-feldspar} + W_{clay} \times (M - m_{SiO_2}) \times P_{Si-clay}}{M} = W_{Si} \tag{6}$$

Formula (6) can be changed to Formula (7):

$$W_{SiO_2} = \frac{m_{SiO_2}}{M} = \frac{W_{Si} - W_{quartz} \times P_{Si-quartz} - W_{plagioclase} \times P_{Si-plagioclase} - W_{K-feldspar} \times P_{Si-K-feldspar} - W_{clay} \times P_{Si-clay}}{P_{Si-SiO_2} - W_{quartz} \times P_{Si-quartz} - W_{plagioclase} \times P_{Si-plagioclase} - W_{K-feldspar} \times P_{Si-K-feldspar} - W_{clay} \times P_{Si-clay}} \tag{7}$$

In Formula (7), only the mass percentage of element Si in clay minerals is difficult to determine, because the molecular formulas of other minerals are known. The molecular formulas of clay

minerals are variable. Therefore, the ideal molecular formulas of different types of clay minerals are applied in this research. For the mass percentage of Si in mixed clay minerals, it is calculated according to the mixed layer ratio based on XRD measurements. Molecular formulas used for kaolinite, montmorillonite, chlorite, and illite are respectively $Al_4(Si_4O_{10})(OH)_8$, $Al_4Si_8O_2(OH)_2$, $Al_6Si_4O_{10}(OH)_8$, and $Al_4(Si_8O_{20})(OH)_4$. The mass percentages of element Si in these are 21.7%, 56.3%, 19.6%, and 31.1%, respectively. The P_{clay} of the tuffaceous shale lithofacies, transitional lithofacies, and carbonate lithofacies samples can be calculated. Then, the contents of amorphous SiO_2 in these samples can be calculated by Formula (7).

4. Results

4.1. Occurrence and Characteristics of Amorphous SiO_2

The shale strata of the Lucaogou Formation in the Jimusar Depression can be divided into tuffaceous shale lithofacies, transitional lithofacies, and carbonate lithofacies [41,42]. The tuffaceous shale lithofacies is mainly composed of feldspathic minerals including quartz and feldspar. The carbonate lithofacies mainly consists of dolomite and includes dolomite and argillaceous dolomite. The mineral composition and lithology of the transitional lithofacies is primarily a hybrid of the other two lithofacies. It can be seen by SEM that in addition to the development of authigenic quartz in the shale strata (Figure 3A,B), amorphous SiO_2 is also present (Figure 3C–H). Amorphous SiO_2 shows no fixed form and usually fills randomly between mineral grains (Figure 3C–E). Some of the amorphous SiO_2 was wrapped in tuffaceous components (Figure 3F), and other forms were spherical or ellipsoid shapes having varying sizes (Figure 3G,H).

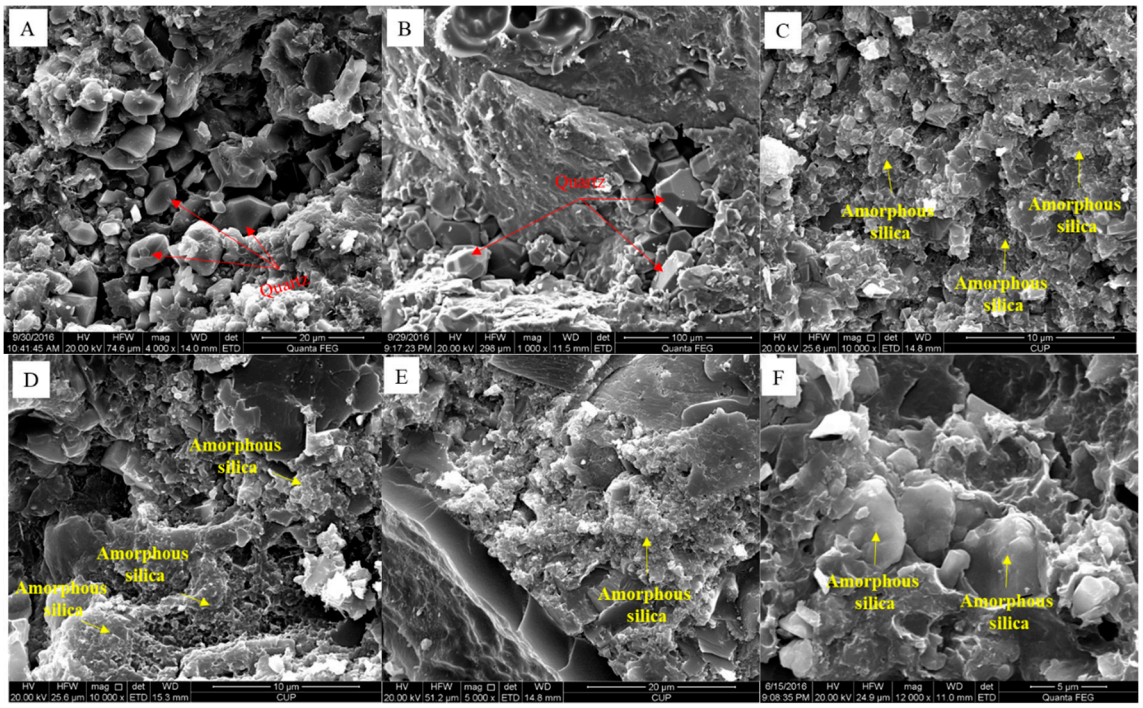

Figure 3. *Cont.*

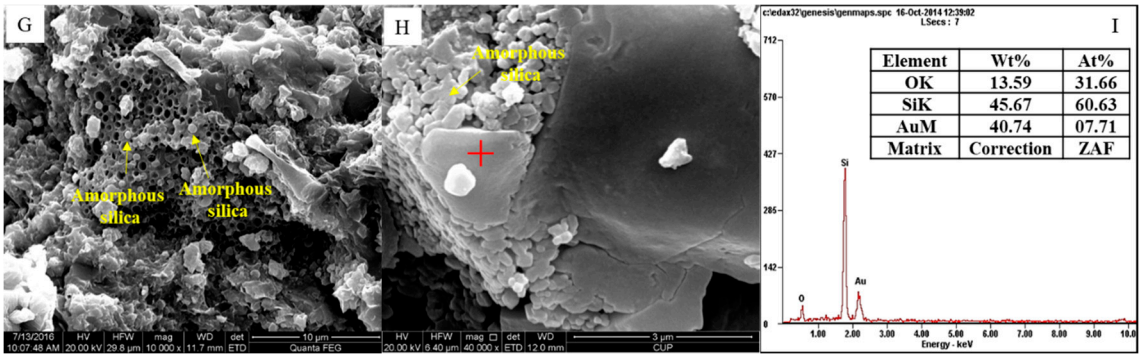

Figure 3. SEM images of quartz and amorphous silica in the Lucaogou Formation, Jimsar Depression. (**A**) Transitional lithofacies, S1 well, 3147.64 m; (**B**) tuffaceous shale lithofacies, S2 well, 3348.08 m; (**C**) transitional lithofacies, S1 well, 3147.64 m; (**D**) tuffaceous shale lithofacies, S2 well, 3343.00 m; (**E**) tuffaceous shale lithofacies, S2 well, 3348.08 m; (**F**) transitional lithofacies, S2 well, 3359.95 m; (**G**) tuffaceous shale lithofacies, S3 well, 2815.21 m; (**H**) tuffaceous shale lithofacies, S4 well, 2601.81 m; (**I**) energy spectrum analysis of point "+" in image H.

4.2. Composition Characteristics of Crystalline Minerals

Analysis of the XRD test results (Table 1) shows that the tuffaceous shale lithofacies samples exhibit the highest content of quartz-feldspathic minerals. The average content of quartz is as much as 40.26%; the average content of plagioclase and k-feldspar are as much as 16.68% and 5.26% respectively (Figure 2A). The carbonate lithofacies samples show the highest content of dolomite, reaching 63% on average. The transitional lithofacies samples present the highest content of clay minerals, which is as much as 26.14% (Figure 2A). In clay minerals, the content of the illite/smectite mixed layer is the highest, followed by illite. The average contents of the illite/smectite mixed layer in tuffaceous shale lithofacies, transitional lithofacies, and carbonate lithofacies are 41.37%, 59.86%, and 72.78%, respectively (Figure 2B). The tuffaceous lithofacies show the highest content of illite (average 37.89%), followed by transitional lithofacies (average 24.29%). The content of kaolinite, chlorite, and chlorite/smectite mixed layer is relatively low (Figure 2B).

4.3. Content of Amorphous SiO_2

Analysis of the XRF test results (Table 2) shows that the tuffaceous shale lithofacies samples have the highest content of Si, reaching 34.21% on average. As expected, the carbonate lithofacies samples exhibit the lowest content of Si, only 11.51% on average (Figure 4A). Moreover, the tuffaceous shale lithofacies samples also exhibit the highest values of Si in crystalline minerals calculated by the above method, reaching 33.18% on average (Figure 4A). According to the calculations, the shale strata of the Lucaogou Formation thereby contains a small amount of amorphous SiO_2. The tuffaceous shale lithofacies samples show the highest content of amorphous SiO_2, reaching an average of 7.07%, and the carbonate lithofacies samples show the lowest, only 1.52% (Figure 4A). Amorphous SiO_2 has a certain negative correlation with crystalline quartz (Figure 4B). During burial diagenesis, amorphous silica will gradually convert to crystalline quartz. The silica in the Lucaogou Formation is mainly derived from tuffaceous materials alteration in previous studies [17,21]. Therefore, the content of amorphous SiO_2 in the tuffaceous shale lithofacies sample is the highest among the three lithofacies. The content of silica in a sample is generally definite. Hence, the higher the content of crystalline quartz, the lower the content of amorphous SiO_2.

Table 1. Test data table of mineral composition of different lithofacies samples in the Luchaogou Formation.

Well	Depth (m)	Lithofacies	Clay Mineral/%	Quartz/%	K-Feldspar /%	Plagioclase/%	Calcite/%	Dolomite/%	Pyrite/%	Kaolinite/%	Chlorite/%	Illite/%	Illite/Smectite Mixed Layers/%	Chlorite/Smectite Mixed Layers/%	Illite/Smectite mixed Layer RATIO/%	Chlorite/Smectite Mixed Layers Ratio/%
S1	3063.80	Carbonate lithofacies	5	19	4	3	8	61	0	5	6	15	74	0	55	0
S1	3086.50	Carbonate lithofacies	2	10	4	5	0	79	0	0	0	50	50	0	56	0
S1	3136.85	Transitional lithofacies	28	22	0	13	3	34	0	8	9	16	67	0	70	0
S1	3147.64	Transitional lithofacies	31	21	4	8	0	33	3	25	29	14	32	0	44	0
S1	3149.00	Carbonate lithofacies	2	5	6	3	0	81	3	3	3	14	80	0	57	0
S2	3343.00	Tuffaceous shale lithofacies	22	23	5	22	0	25	3	0	0	64	36	0	40	0
S2	3315.00	Carbonate lithofacies	3	12	0	18	13	53	1	5	4	10	81	0	50	0
S2	3323.00	Transitional lithofacies	23	28	0	17	3	27	2	0	6	10	35	49	67	60
S2	3332.00	Carbonate lithofacies	2	13	0	18	5	60	2	9	6	9	76	0	49	0
S2	3344.00	Transitional lithofacies	17	17	9	12	7	35	3	0	11	24	65	0	56	0
S2	3347.00	Transitional lithofacies	39	26	0	10	10	12	3	0	7	15	78	0	55	0
S2	3348.08	Tuffaceous shale lithofacies	22	31	8	12	0	23	4	0	0	85	15	0	40	0
S2	3351.66	Carbonate lithofacies	2	19	0	10	24	45	0	4	4	32	60	0	52	0

Table 1. *Cont.*

Well	Depth (m)	Lithofacies	Clay Mineral/%	Quartz/%	K-Feldspar /%	Plagioclase/%	Calcite/%	Dolomite/%	Pyrite/%	Kaolinite/%	Chlorite/%	Illite/%	Illite/Smectite Mixed Layers/%	Chlorite/Smectite Mixed Layers/%	Illite/Smectite mixed Layer RATIO/%	Chlorite/Smectite Mixed Layers Ratio/%
S2	3353.14	Carbonate lithofacies	2	10	1	14	2	71	0	8	9	28	55	0	56	0
S2	3355.13	Transitional lithofacies	32	21	0	11	0	33	3	0	0	43	57	0	54	0
S2	3359.95	Transitional lithofacies	22	14	8	14	6	36	0	2	2	81	15	0	67	0
S2	3379.55	Transitional lithofacies	23	20	7	16	4	25	5	0	8	9	83	0	61	0
S2	3380.01	Tuffaceous shale lithofacies	16	48	11	20	0	0	5	12	15	0	73	0	90	0
S2	3463.00	Transitional lithofacies	27	15	6	14	0	36	2	0	0	38	62	0	51	0
S2	3477.00	Transitional lithofacies	26	20	9	14	0	28	3	0	7	13	80	0	65	0
S2	3600.34	Carbonate lithofacies	4	10	9	8	6	60	3	3	3	15	79	0	49	0
S3	2794.71	Tuffaceous shale lithofacies	18	40	4	21	12	4	1	13	15	9	63	0	87	0
S3	2795.80	Tuffaceous shale lithofacies	14	59	3	4	8	12	0	0	0	80	20	0	40	0
S3	2805.21	Transitional lithofacies	12	15	0	27	0	43	3	5	6	0	89	0	70	0
S3	2808.52	Carbonate lithofacies	7	6	10	10	10	57	0	0	0	0	100	0	52	0

Table 1. *Cont.*

Well	Depth (m)	Lithofacies	Clay Mineral/%	Quartz/%	K-Feldspar /%	Plagioclase/%	Calcite/%	Dolomite/%	Pyrite/%	Kaolinite/%	Chlorite/%	Illite/%	Illite/Smectite Mixed Layers/%	Chlorite/Smectite Mixed Layers/%	Illite/Smectite mixed Layer RATIO/%	Chlorite/Smectite Mixed Layers Ratio/%
S3	2815.21	Tuffaceous shale lithofacies	27	30	9	18	6	5	5	0	0	94	6	0	40	0
S3	2817.81	Tuffaceous shale lithofacies	18	54	0	17	4	4	3	11	12	8	69	0	89	0
S3	2832.89	Tuffaceous shale lithofacies	22	38	7	10	19	1	3	0	0	98	2	0	40	0
S3	2857.65	Tuffaceous shale lithofacies	22	40	13	15	3	2	5	0	0	95	5	0	40	0
S3	2869.14	Tuffaceous shale lithofacies	23	38	8	5	0	26	0	0	0	86	14	0	40	0
S3	2870.01	Tuffaceous shale lithofacies	19	37	10	15	5	11	3	23	18	0	59	0	85	0
S3	2871.01	Tuffaceous shale lithofacies	18	35	13	23	3	4	4	14	17	0	69	0	88	0
S3	2873.01	Tuffaceous shale lithofacies	18	36	0	26	6	11	3	15	14	6	65	0	83	0
S3	2874.01	Tuffaceous shale lithofacies	23	38	0	26	4	5	4	14	16	0	70	0	86	0

Table 1. *Cont.*

Well	Depth (m)	Lithofacies	Clay Mineral/%	Quartz/%	K-Feldspar /%	Plagioclase/%	Calcite/%	Dolomite/%	Pyrite/%	Kaolinite/%	Chlorite/%	Illite/%	Illite/Smectite Mixed Layers/%	Chlorite/Smectite Mixed Layers/%	Illite/Smectite mixed Layer RATIO/%	Chlorite/Smectite Mixed Layers Ratio/%
S3	2876.81	Tuffaceous shale lithofacies	22	41	0	19	6	9	3	8	7	4	0	81	0	50
S4	2580.81	Transitional lithofacies	25	20	0	16	0	37	2	12	11	49	28	0	40	0
S4	2585.01	Transitional lithofacies	21	15	8	14	0	37	5	4	6	28	62	0	59	0
S4	2591.91	Tuffaceous shale lithofacies	21	51	0	13	8	5	2	13	16	4	67	0	86	0
S4	2592.21	Tuffaceous shale lithofacies	26	36	0	26	0	9	3	16	18	6	60	0	86	0
S4	2601.21	Tuffaceous shale lithofacies	17	50	3	15	8	3	4	12	14	7	67	0	86	0
S4	2601.81	Tuffaceous shale lithofacies	16	40	6	10	21	3	4	0	0	74	26	0	40	0
S4	2607.60	Transitional lithofacies	40	36	3	3	0	12	6	15	0	0	85	0	60	0

Table 2. Statistical table of calculated silica content, porosity, permeability, mechanical properties, and oil saturation in different lithofacies samples of the Lucaogou Formation.

Well	Depth (m)	Lithofacies	Oil Saturation/%	Young's Modulus/N*mm^{-2}	Poisson's Ratio	Compressive Strength/Kg*cm^{-2}	Porosity/%	Permeability/mD	Si Content Test by XRF/%	Amorphous Silica Content Calculated Through the New Method/%	Calculated Si Content in Crystalline Minerals/%	Calculated Si Content in Clay Minerals/%
S1	3063.80	Carbonate lithofacies	17.6	–	–	–	–	–	13.535	1.017	13.184	40.196
S1	3086.50	Carbonate lithofacies	10.9	–	–	–	0.7041	0.0013	9.197	2.410	8.246	38.156
S1	3136.85	Transitional lithofacies	–	–	–	–	–	–	26.937	4.652	25.924	41.131
S1	3147.64	Transitional lithofacies	9.70	–	–	–	0.2367	0.0000923	24.348	6.921	22.612	28.963
S1	3149.00	Carbonate lithofacies	–	–	–	–	0.6041	0.00215	7.013	2.540	5.939	41.964
S2	3343.00	Tuffaceous shale lithofacies	5.80	–	–	–	0.5851	0.000043	29.234	11.885	26.743	34.728
S2	3315.00	Carbonate lithofacies	14.4	6.396	0.211	306.527	–	–	12.545	0.542	12.353	40.376
S2	3323.00	Transitional lithofacies	15.40	36.212	0.246	196.722	–	–	25.334	2.878	24.671	26.948
S2	3332.00	Carbonate lithofacies	1	16.381	0.353	368.663	1.1986	0.01	12.978	1.643	12.398	38.948
S2	3344.00	Transitional lithofacies	12.00	–	–	–	–	–	21.979	3.412	21.070	39.007
S2	3347.00	Transitional lithofacies	26.10	10.707	0.308	94.94	–	–	31.536	0.570	31.443	41.105
S2	3348.08	Tuffaceous shale lithofacies	–	40.386	0.356	324.954	–	–	30.056	10.484	27.990	32.612

Table 2. *Cont.*

Well	Depth (m)	Lithofacies	Oil Saturation/%	Young's Modulus/N*mm^{-2}	Poisson's Ratio	Compressive Strength/Kg*cm^{-2}	Porosity/%	Permeability/mD	Si Content Test by XRF/%	Amorphous Silica Content Calculated Through the New Method/%	Calculated Si Content in Crystalline Minerals/%	Calculated Si Content in Clay Minerals/%
S2	3351.66	Carbonate lithofacies	–	12.181	0.225	234.695	0.9727	0.00236	13.028	0.472	12.836	38.126
S2	3353.14	Carbonate lithofacies	22.7	–	–	–	–	–	10.224	0.522	10.027	37.074
S2	3355.13	Transitional lithofacies	9.90	35.739	0.333	173.612	–	–	26.256	2.251	25.762	38.856
S2	3359.95	Transitional lithofacies	–	–	–	–	–	–	22.943	8.594	20.615	33.214
S2	3379.55	Transitional lithofacies	8.60	14.625	0.202	184.049			26.952	2.838	26.346	42.938
S2	3380.01	Tuffaceous shale lithofacies	–	–	–	–	–	–	39.916	6.143	39.407	44.803
S2	3463.00	Transitional lithofacies	–	–	–	–	0.4650	0.0109	25.431	7.099	23.729	39.068
S2	3477.00	Transitional lithofacies	–	18.328	0.269	114.190	1.1957	0.135	28.659	4.529	27.756	43.399
S2	3600.34	Carbonate lithofacies	2.10	26.013	0.317	373.744	–	–	12.147	1.773	11.505	40.227
S3	2794.71	Tuffaceous shale lithofacies	40.90	35.675	0.244	178.849	1.2807	0.012	34.525	2.676	34.163	41.965
S3	2795.80	Tuffaceous shale lithofacies	32.10	26.702	0.241	139.743	1.1727	0.0162	35.295	3.167	34.889	33.116
S3	2805.21	Transitional lithofacies	–	–	–	–	0.6000	0.0244	22.358	5.936	20.759	45.639
S3	2808.52	Carbonate lithofacies	–	12.089	0.271	319.996	0.9194	0.00105	12.957	2.718	11.986	44.204

Table 2. *Cont.*

Well	Depth (m)	Lithofacies	Oil Saturation/%	Young's Modulus/N*mm^{-2}	Poisson's Ratio	Compressive Strength/Kg*cm^{-2}	Porosity/%	Permeability/mD	Si Content Test by XRF/%	Amorphous Silica Content Calculated Through the New Method/%	Calculated Si Content in Crystalline Minerals/%	Calculated Si Content in Clay Minerals/%
S3	2815.21	Tuffaceous shale lithofacies	8.90	–	–	–	0.9194	0.00244	32.932	11.535	31.006	31.704
S3	2817.81	Tuffaceous shale lithofacies	70.30	13.176	0.278	67.705	1.8524	0.0301	38.87632	0.589	38.824	44.161
S3	2832.89	Tuffaceous shale lithofacies	–	–	–	–	–	–	31.874	9.893	30.136	31.301
S3	2857.65	Tuffaceous shale lithofacies	36.60	–	–	–	–	–	35.511	7.841	34.474	31.604
S3	2869.14	Tuffaceous shale lithofacies	13.20	39.502	0.293	181.272	1.4511	0.076	31.016	8.205	29.524	32.511
S3	2870.01	Tuffaceous shale lithofacies	31.80	–	–	–	–	–	33.429	4.922	32.690	39.505
S3	2871.01	Tuffaceous shale lithofacies	–	18.927	0.327	128.162	–	–	36.128	6.621	35.307	43.130
S3	2873.01	Tuffaceous shale lithofacies	–	–	–	–	–	–	33.013	3.377	32.499	41.675
S3	2874.01	Tuffaceous shale lithofacies	–	35.684	0.355	132.212	–	–	36.425	4.705	35.868	43.114
S3	2876.81	Tuffaceous shale lithofacies	31.50	33.164	0.192	276.39	–	–	30.243	9.486	28.413	14.260
S4	2580.81	Transitional lithofacies	1.70	39.594	0.287	435.174	0.5100	0.000089	23.923	6.616	22.238	31.529
S4	2585.01	Transitional lithofacies	–	–	–	–	0.5600	0.043	22.973	3.681	22.027	39.252

Table 2. *Cont.*

Well	Depth (m)	Lithofacies	Oil Saturation/%	Young's Modulus/N*mm^{-2}	Poisson's Ratio	Compressive Strength/Kg*cm^{-2}	Porosity/%	Permeability/mD	Si Content Test by XRF/%	Amorphous Silica Content Calculated Through the New Method/%	Calculated Si Content in Crystalline Minerals/%	Calculated Si Content in Clay Minerals/%
S4	2591.91	Tuffaceous shale lithofacies	29.00	–	–	–	–	–	37.636	4.359	37.177	42.558
S4	2592.21	Tuffaceous shale lithofacies	–	–	–	–	–	–	35.947	3.382	35.535	40.529
S4	2601.21	Tuffaceous shale lithofacies	56.20	31.654	0.396	148.228	–	–	36.932	3.331	36.561	42.882
S4	2601.81	Tuffaceous shale lithofacies	–	–	–	–	–	–	31.012	9.318	29.297	33.721
S4	2607.60	Transitional lithofacies	9.10	–	–	–	1.1364	0.05	36.134	1.164	35.998	42.542

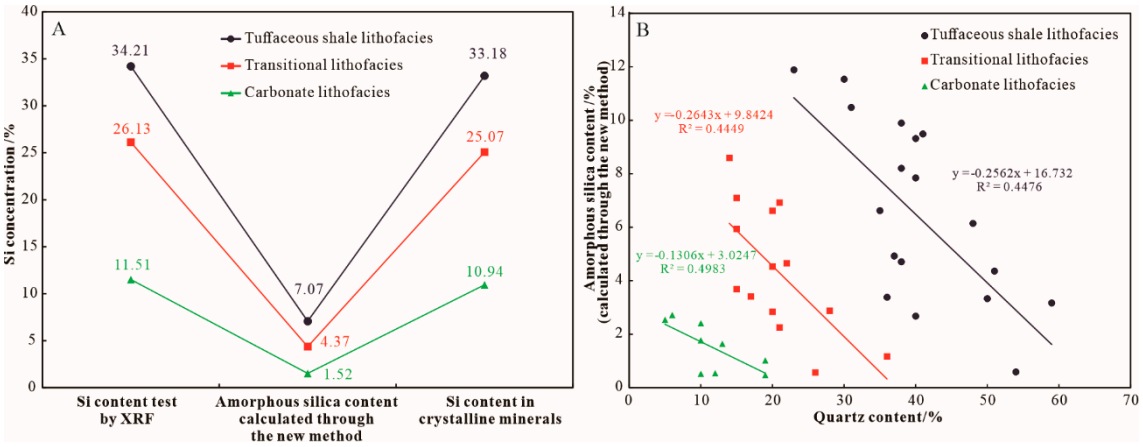

Figure 4. Diagrams showing (**A**) Si content tested by XRF, amorphous silica content calculated through the new method, and Si content in crystalline minerals. (**B**) cross plot of the amorphous silica content with crystalline quartz content in samples of the different lithofacies in the Lucaogou Formation.

5. Discussion

5.1. Advantages and Disadvantages of the New Method

Compared with the previous quantitative analysis methods for amorphous SiO_2, the new method does not require chemical dissolution. The most important is that the cost of this method is much lower. The equipment required has already been widely used for a large-scale sample testing. This method also has some shortcomings: the ideal formula of clay mineral is used to calculate the mass percentage of elemental Si in clay minerals. Using illite as an example, its ideal structural molecular formula is $Al_4(Si_8O_{20})(OH)_4$, and the mass percentage of Si is 31.1%. However, due to the fact that the illite in the actual sample contains impurities, its molecular formula is diverse, which introduces small errors into the calculated value.

5.2. The Influence of Amorphous SiO_2 on Reservoir Properties

The silica content is mainly derived from the alteration of tuffaceous material in the shale strata. It was found through the cross plot between the calculated amorphous SiO_2 content and the reservoir physical property data that amorphous SiO_2 content was negatively correlated with reservoir porosity and permeability (Figure 5). The content of amorphous SiO_2 is negatively correlated with the content of crystalline quartz (Figure 4B). Hence, it indicates that the higher the content of crystalline quartz, the higher the porosity and permeability of the reservoir. Alteration is an important cause of pore formation in the Lucaogou Formation because it is a process of volume reduction for the total material [43,44]. From the perspective of density, it is easy to understand this process of volume reduction. The density of volcanic ash is only 2.3 g/cm^3, while the mineral density after its alteration is much higher than 2.3 g/cm^3, such as quartz 2.6–2.7 g/cm^3. According to the law of conservation of mass, the overall volume must decrease. In other words, a large amount of silica was released during the alteration of tuffaceous components. Some silica crystallized to authigenic quartz, which increases the physical properties of the reservoir, while some silica did not crystallize and occurs between the grains in the form of amorphous SiO_2 cement, which reduces the storage space of the reservoir.

The rock mechanical parameters of the Lucaogou Formation were measured by triaxial stress experiment under given confining pressure (Table 2). The calculated content of amorphous SiO_2 was positively correlated with Young's modulus and compressive strength (Figure 6A,B). It indicates that the higher the content of amorphous SiO_2 was, the harder the samples were to be deformed and fractured. Amorphous SiO_2 cements various grains together, making the reservoir more compacted. Amorphous SiO_2 is negatively correlated with oil saturation (Figure 6D). It indicates that the existence of amorphous SiO_2 is unfavorable for hydrocarbon enrichment. Previous studies suggested that volcanic

ash would lead to algal blooms, and the alteration of volcanic ash would also generate a large number of pore spaces, which provided storage space for hydrocarbon enrichment. During volcanic eruptions, a large amount of volcanic ash was deposited with particulate organic matter and well preserved in a strong reduction environment. At last, they further condensed into kerogen and became source rocks with high organic matter. The organic matter type of Lucaogou Formation shale is mainly I~II_1 type, which suggests an origin of bacteria, algae, and other aquatic organisms [19]. However, the presence of amorphous SiO_2 makes the tuffaceous shale lithofacies lack sufficient storage space. Furthermore, part of hydrocarbon migrated to the adjacent carbonate lithofacies. On the whole, amorphous SiO_2 in Lucaogou Formation in Jimsar Depression is not high in content (Figure 4A and Table 2), which is merely the same to that of K-feldspar. Therefore, the changes in reservoir properties are likely to be caused by other factors, such as the development of laminae, the direction of stress in triaxial stress experiments, and so on. In the early diagenetic stage (Ro is 0.35%~0.5%), amorphous SiO_2 has already started to crystallize to quartz in large quantities [23,24]. It can be inferred that the amorphous SiO_2 should have a greater physical influence on shale samples in the earlier diagenetic stage.

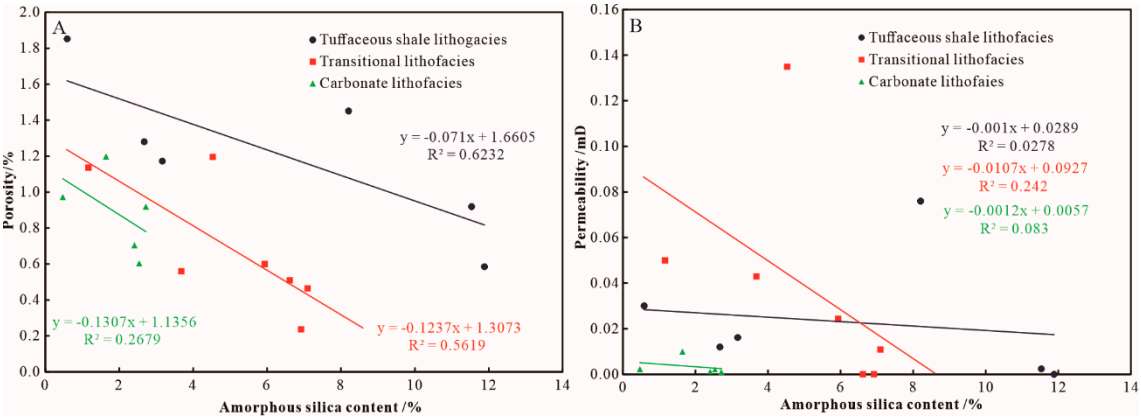

Figure 5. Cross plot of amorphous silica content with (**A**) porosity, (**B**) permeability of different lithofacies in Lucaogou Formation.

5.3. Factors Controlling the Conversion of Amorphous SiO_2 into Quartz

The conversion of amorphous SiO_2 into quartz in diagenesis was affected by many factors, including temperature, properties of fluid medium, burial, and formation pressure, etc. [45–48]. It was proposed that the hydrocarbon injection and formation overpressure can inhibit the formation of authigenic quartz [46–48]. However, in the same one sample, both authigenic quartz and amorphous SiO_2 occur (Figures 3 and 7), the contents of amorphous silica in the four samples (Figure 7A–D) are 6.921%, 10.484%, 11.535%, and 9.318% (Table 2). It means temperature, fluid properties, and formation pressure was not the key factor. It was found that authigenic quartz tended to develop in pores, holes, or fractures through a large number of scanning electron microscope observations (Figure 7). It was a reasonable presumption that the authigenic quartz can only grow when there was space. Without growth space, it can only be amorphous SiO_2 without crystal morphological characteristics. The silica in shale strata of Lucaogou Formation mainly came from the tuffaceous material alteration. A large amount of silica was released. When these pores were filled with a large amount of amorphous SiO_2, there was no room left for the growth of the authigenic quartz. Hence, the amorphous SiO_2 merely existed in the amorphous state. Only when the silica-rich fluid entered one of those large pores, holes, or cracks was there enough space for silica to grow to authigenic quartz.

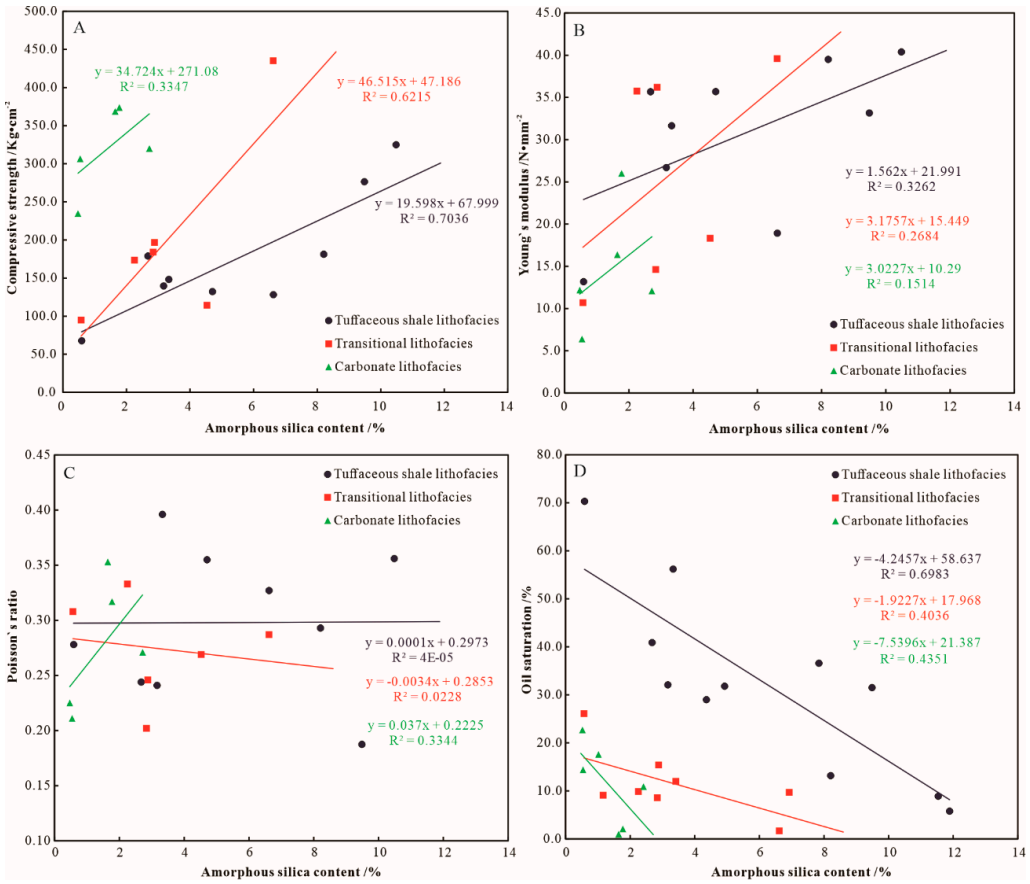

Figure 6. Cross plot of amorphous silica content with (**A**) Young's modulus, (**B**) Poisson's ratio, (**C**) compressive strength and (**D**) oil saturation of different lithofacies in Lucaogou Formation.

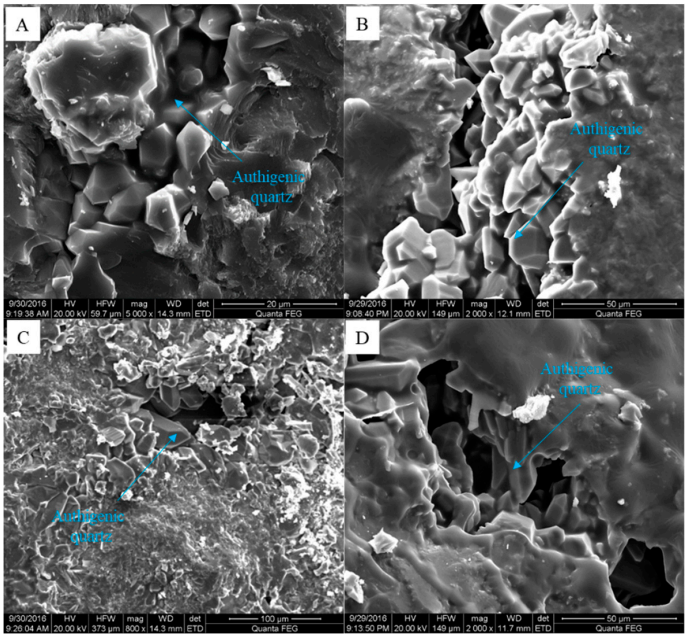

Figure 7. Scanning electron microscope of authigenic quartz in the pores, cavities, and cracks of Lucaogou Formation. (**A**) Transitional lithofacies, S1 well, 3147.64 m; (**B**) tuffaceous shale lithofacies, S2 well, 3348.08 m; (**C**) tuffaceous shale lithofacies, S3 well, 2815.21 m; (**D**) tuffaceous shale lithofacies, S4 well, 2601.81 m.

6. Conclusions

The amorphous SiO_2 in the shale strata of the Lucaogou Formation of the Jimusar Depression had no specific form and was usually mounded among mineral grains. XRD analysis measured the percentage of crystalline minerals, while XRF measured the percentage of elemental Si. Therefore, a new quantitative analysis method for calculating the percentage of amorphous SiO_2 was established by combining the two methods. The content of amorphous SiO_2 in the tuffaceous shale lithofacies of the Lucaogou Formation was the highest, with an average of 7.07%.

The calculation confirmed that the higher the content of amorphous SiO_2, the lower the porosity of the reservoir. Moreover, amorphous SiO_2 was found to be inversely proportional to the compressive strength, Young's modulus, and oil saturation of the reservoir. It indicates that amorphous SiO_2 reduces the physical properties of the reservoir, increases the plasticity, and increases the difficulty of fracturing during development for hydrocarbon extraction. The lack of growing space is the key factor affecting the conversion of amorphous SiO_2 into crystalline quartz. Thus, the existence of amorphous SiO_2 is harmful to shale reservoirs in many ways and has economic impact deleterious to oil and gas exploration and development.

Author Contributions: Conceptualization, Q.C.; methodology, K.S.; software, K.S. and C.C.; investigation, K.S.; resources, Q.C. and G.C.; writing—original draft preparation, K.S.; writing—review and editing, K.S., Y.L., G.C. and C.C.; supervision, Q.C. and G.C.; project administration, Q.C. and G.C. All authors have read and agreed to the published version of the manuscript.

Funding: This research was funded by National Science and Technology Major Project Foundation of China (2016ZX05006-003-002; 2016ZX05014-002); National Nature Science Foundation of China (41802157); Fundamental Research Funds for the Central Universities, China University of Geoscience (Wuhan) (102-162301202627); China Postdoctoral Science Foundation (2016M592265).

Conflicts of Interest: The authors declare no conflict of interest.

References

1. Zhang, J.C.; Xu, B.; Nie, H.K.; Wang, Z.Y.; Lin, T. Exploration potential of shale gas resources in China. *Natl. Gas Ind.* **2008**, *28*, 136–140.
2. Guo, T.L.; Zhang, H.R. Formation and enrichment mode of Jiaoshiba shale gas field, Sichuan Basin. *Pet. Explor. Dev.* **2014**, *41*, 31–40. [CrossRef]
3. Zou, C.; Zhao, Q.; Dong, D.; Yang, Z.; Qiu, Z.; Liang, F.; Wang, N.; Huang, Y.; Duan, A.; Zhang, Q.; et al. Geological characteristics, main challenges and future prospect of shale gas. *J. Natl. Gas Geosci.* **2017**, *2*, 273–288. [CrossRef]
4. Jin, Z.J.; Nie, H.K.; Liu, Q.Y.; Zhao, J.H.; Jiang, T. Source and seal coupling mechanism for shale gas enrichment in upper Ordovician Wufeng Formation—Lower Silurian Longmaxi Formation in Sichuan Basin and its periphery. *Mar. Pet. Geol.* **2018**, *97*, 78–93. [CrossRef]
5. Chen, X.; Fan, J.X.; Wang, W.H.; Wang, H.Y.; Nie, H.K.; Shi, X.W.; Wen, Z.D.; Chen, D.Y.; Li, W.J. Stage-progressive distribution pattern of the Lungmachi black graptolitic shales from Guizhou to Chongqing, Central China. *Sci. China Earth Sci.* **2017**, *60*, 1133–1146. [CrossRef]
6. Bowker, K.A. Barnett Shale gas production, Fort Worth Basin: Issues and discussion. *AAPG Bull.* **2007**, *91*, 523–533. [CrossRef]
7. Jarvie, D.M.; Hill, R.J.; Ruble, T.E.; Pollastro, R.M. Unconventional shale-gas systems: The Mississippian Barnett shale of north-central Texas as one model for thermo-genic shale-gas assessment. *AAPG Bull.* **2007**, *91*, 475–499. [CrossRef]
8. Ruyue, W.; Wenlong, D.; Dajian, G.; Jigao, L.; Xinghua, W.; Shuai, Y. Gas preservation conditions of marine shale in northern Guizhou area: A case study of the Lower Cambrian Niutitang Formation in the Cen'gong block, Guizhou Province. *Oil Gas Geol.* **2016**, *37*, 45–55.

9. Wang, R.; Hu, Z.; Sun, C.; Liu, Z.; Zhang, C.; Gao, B.; Du, W.; Zhao, J.; Tang, W. Comparative analysis and discussion of shale reservoir characteristics in the Wufeng-Longmaxi and Niutitang formations. *Pet. Geol. Exp.* **2018**, *40*, 639–649.
10. Dong, T.; Harris, N.B.; Ayranci, K.; Yang, S. The impact of rock composition on geomechanical properties of a shale formation: Middle and Upper Devonian Horn River Group shale, Northeast British Columbia, Canada. *AAPG Bull.* **2017**, *101*, 177–204. [CrossRef]
11. Guo, X.S.; Hu, D.F.; Wen, Z.D.; Liu, R.B. Major factors controlling the accumulation and high productivity in marine shale gas in the Lower Paleozoic of Sichuan Basin and its periphery: A case study of the Wufeng-Longmaxi Formation of Jiaoshiba area. *Geol. China* **2014**, *41*, 893–901.
12. Lu, L.; Qin, J.; Shen, B.; Teng, G.; Liu, W.; Zhang, Q. Biogenic origin and hydrocarbon significance of siliceous shale from the Wufeng-Longmaxi formations in Fuling area, southeastern Sichuan Basin. *Pet. Geol. Exp.* **2016**, *38*, 460–472.
13. Lu, L.; Qin, J.; Shen, B.; Teng, G.; Liu, W.; Zhang, Q. The origin of biogenic silica in siliceous shale from Wufeng-Longmaxi Formation in the Middle and Upper Yangtze region and its relationship with shale gas enrichment. *Earth Sci. Front.* **2018**, *25*, 226–236.
14. Zhao, J.; Jin, Z.; Jin, Z.; Wen, X.; Geng, Y.K.; Yan, C.N. The genesis of quartz in Wufeng-Longmaxi gas shales, Sichuan Basin. *Natl. Gas Geosci.* **2016**, *27*, 377–386.
15. Wang, S.; Zou, C.; Dong, D.; Wang, Y.; Huang, J.; Guo, Z. Biogenic silica of organic-rich shale in Sichuan Basin and its significance for shale gas. *Acta Sci. Nat. Univ. Pekin.* **2014**, *50*, 476–486.
16. Liu, G.; Zhai, G.; Zou, C.; Cheng, L.; Guo, X.; Xia, X.; Shi, D.; Yang, Y.; Zhang, C.; Zhou, Z. A comparative discussion of the evidence for biogenic silica in Wufeng-Longmaxi siliceous shale reservoir in the Sichuan basin, China. *Mar. Pet. Geol.* **2019**, *109*, 70–87. [CrossRef]
17. Liu, G.; Zhai, G.; Huang, Z.; Zou, C.; Xia, X.; Shi, D.; Zhou, Z.; Zhang, C.; Chen, R.; Yu, S.; et al. The effect of tuffaceous material on characteristics of different lithofacies: A case study on Lucaogou Formation fine-grained sedimentary rocks in Santanghu Basin. *J. Pet. Sci. Eng.* **2019**, *179*, 355–377. [CrossRef]
18. Xianzheng, Z.H.; Lihong, Z.H.; Xiugang, P.U.; Fengming, J.; Wenzhong, H.; Dunqing, X.; Shiyue, C.H.; Zhannan, S.H.; Zhang, W.; Fei, Y.A. Geological characteristics of shale rock system and shale oil exploration breakthrough in a lacustrine basin: A case study from the Paleogene 1st sub-member of Kong 2 Member in Cangdong sag, Bohai Bay Basin, China. *Pet. Explor. Dev.* **2018**, *45*, 377–388.
19. Liu, G.; Liu, B.; Huang, Z.; Chen, Z.; Jiang, Z.; Guo, X.; Li, T.; Chen, L. Hydrocarbon distribution pattern and logging identification in lacustrine fine-grained sedimentary rocks of the Permian Lucaogou Formation from the Santanghu basin. *Fuel* **2018**, *222*, 207–231. [CrossRef]
20. Liu, G.H.; Huang, Z.L.; Guo, X.B.; Liu, Z.Z.; Gao, X.Y.; Chen, C.C.; Zhang, C.L. The research of SiO_2 occurrence in mud shale reservoir of the Yanchang formation in Ordos Basin. *Acta Geol. Sin.* **2016**, *90*, 1016–1029.
21. Liu, G.H.; Huang, Z.L.; Guo, X.B.; Liu, Z.Z.; Gao, X.Y.; Chen, C.C.; Zhang, C.L. The SiO_2 occurrence and origin in the shale system of middle Permian series Lucaogou Formation in Malang Sag, Santanghu Basin, Xinjiang. *Acta Geol. Sin.* **2016**, *90*, 1220–1235.
22. Huang, Z.; Liu, G.; Li, T.; Li, Y.; Yin, Y.; Wang, L. Characterization and control of mesopore structural heterogeneity for low thermal maturity shale: A case study of Yanchang Formation shale, Ordos Basin. *Energy Fuels* **2017**, *31*, 11569–11586. [CrossRef]
23. Zhao, J.; Jin, Z.; Jin, Z.; Hu, Q.; Hu, Z.; Du, W.; Yan, C.; Geng, Y. Mineral types and organic matters of the Ordovician-Silurian Wufeng and Longmaxi Shale in the Sichuan Basin, China: Implications for pore systems, diagenetic pathways, and reservoir quality in fine-grained sedimentary rocks. *Mar. Pet. Geol.* **2017**, *86*, 655–674. [CrossRef]
24. Zhao, J.; Jin, Z.; Jin, Z.; Wen, X.; Geng, Y. Origin of authigenic quartz in organic-rich shales of the Wufeng and Longmaxi Formations in the Sichuan Basin, South China: Implications for pore evolution. *J. Natl. Gas Sci. Eng.* **2017**, *38*, 21–38. [CrossRef]
25. Zhang, L.; Li, B.; Jiang, S.; Xiao, D.; Lu, S.; Zhang, Y.; Gong, C.; Chen, L. Heterogeneity characterization of the lower Silurian Longmaxi marine shale in the Pengshui area, South China. *Int. J. Coal Geol.* **2018**, *195*, 250–266. [CrossRef]

26. Peltonen, C.; Marcussen, Ø.; Bjørlykke, K.; Jahren, J. Clay mineral diagenesis and quartz cementation in mudstones: The effects of smectite to illite reaction on rock properties. *Mar. Pet. Geol.* **2009**, *26*, 887–898. [CrossRef]
27. Thyberg, B.; Jahren, J.; Winje, T.; Bjørlykke, K.; Faleide, J.I.; Marcussen, Ø. Quartz cementation in Late Cretaceous mudstones, northern North Sea: Changes in rock properties due to dissolution of smectite and precipitation of microquartz crystals. *Mar. Pet. Geol.* **2010**, *27*, 1752–1764. [CrossRef]
28. Thyberg, B.; Jahren, J. Quartz cementation in mudstones: Sheet-like quartz cement from clay mineral reactions during burial. *Pet. Geosci.* **2011**, *17*, 53–63. [CrossRef]
29. Chaika, C.; Williams, L.A. Density and mineralogy variations as a function of porosity in Miocene Monterey Formation oil and gas reservoirs in California. *AAPG Bull.* **2001**, *85*, 149–167.
30. Lin, J.H. Quantitative analysis of amorphous silica in multicomponent system by X-ray diffraction. *J. Mineral. Petrol.* **1997**, *17*, 22–25.
31. Liu, G.H. The Formation Mechanism of Authigenic Quartz in Lacustrine Shale and Influence to Reservoir Property [D]. Ph.D. Thesis, China University of Petroleum, Beijing, China, 2017.
32. Chu, G. A Doping Method for Quantitative X-Ray Diffraction Phase Analysis of Samples Containing Amorphous Material. *Acta Phys. Sin.* **1998**, *47*, 1143–1148.
33. Popović, S.; Gržeta-plenković, B.; Balić-žunić, T. The doping method in quantitative x-ray diffraction pahase analysis addendum. *J. Appl. Crystallogr.* **1983**, *16*, 505–507. [CrossRef]
34. Huang, Z.; Liu, G.; Ma, J.; Xue, D.; Han, W.; Chen, J.; Chen, Z. A new method for semiquantitative analysis of amorphous SiO_2 in terrestrial shale: A case study about Yanchang Formation shale, Ordos Basin. *Natl. Gas Geosci.* **2015**, *26*, 2017–2028.
35. Cao, Z.; Liu, G.; Kong, Y.; Wang, C.; Niu, Z.; Zhang, J.; Wei, Z. Lacustrine tight oil accumulation characteristics: Permian Lucaogou Formation in jimusaer sag, Junggar Basin. *Int. J. Coal Geol.* **2016**, *153*, 37–51. [CrossRef]
36. Qu, C.S.; Qiu, L.W.; Cao, Y.C. Organic petrology characteristics and occurrence of source rocks in Permian Lucaogou Formation, Jimsar sag. *J. China Univ. Pet. (Ed. Natl. Sci.)* **2017**, *41*, 30–38.
37. Zhou, D.W.; Liu, Y.Q.; Xing, X.J.; Hao, J.R.; Dong, Y.P.; Ouyang, Z.J. Formation of the Permian basalts and implications of geochemical tracing for paleo-tectonic setting and regional tectonic background in the Turpan-Hami and Santanghu basins, Xinjiang. *Sci. China Ser. D* **2006**, *49*, 584–596. [CrossRef]
38. Jiang, Y.Q.; Liu, Y.Q.; Zhao, Y.; Nan, Y.; Wang, R.; Zhou, P.; Yang, Y.J.; Kou, J.Y.; Zhou, N.C. Characteristics and origin of tuff-type tight oil in Jimusar sag, Junggar Basin, NW China. *Pet. Explor. Dev.* **2015**, *42*, 810–818. [CrossRef]
39. Wang, J.; Zhou, L.; Liu, J.; Zhang, X.J.; Zhang, F.; Zhang, B. Acid-base alternation diagenesis and its influence on shale reservoirs in the Permian Lucaogou Formation, Jimusar Sag, Junggar Basin, NW China. *Pet. Explor. Dev.* **2020**, *47*, 962–976. [CrossRef]
40. Liu, C.; Liu, K.; Wang, X.; Wu, L.; Fan, Y. Chemostratigraphy and sedimentary facies analysis of the Permian Lucaogou Formation in the Jimusaer Sag, Junggar Basin, NW China: Implications for tight oil exploration. *J. Asian Earth Sci.* **2019**, *178*, 96–111. [CrossRef]
41. Wang, C.Y.; Kuang, L.C.; Gao, G.; Cui, W.; Kong, Y.H.; Xiang, B.L.; Liu, G.D. Difference in hydrocarbon generation potential of the shaly source rocks in Jimusar sag' Permian Lucaogou formation. *Acta Sedimentol. Sin.* **2014**, *32*, 385–390.
42. Zhi, Y.; Lianhua, H.; Senhu, L.; Xia, L.; Lijun, Z.; Songtao, W.; Jingwei, C. Geologic characteristics and exploration potential of tight oil and shale oil in Lucaogou formation in Jimsar sag. *China Pet. Explor.* **2018**, *23*, 76–85.
43. Cai, D.M.; Sun, L.D.; Qi, J.S.; Dong, J.H.; Zhu, Y.K. Reservoir characteristics and evolution of volcanic rocks in Xujiaweizi fault depression. *Acta Pet. Sin.* **2010**, *31*, 400–407.
44. Hu, W.T.; Liu, C.Z.; Zhao, H.; Luan, K.; Yao, H.P. The Diagenesis of Volcanic Rocks and Its Effects on the Reservior Quality in Xujiaweizi Fault Depression, Soliao Basin. *Sci. Technol. Eng.* **2011**, *11*, 1176–1181.
45. Yang, J.S.; Meng, Y.L.; Zhang, H. Kinetic model of quartz cementation and its application. *Pet. Geol. Exp.* **2002**, *24*, 372–376.
46. Yuan, D.S.; Zhang, Z.H.; Zhu, L.; Liu, H.J. Effects of oil charge on quartz cement. *Acta Petrol. Sin.* **2007**, *23*, 2315–2320.

47. Li, R.; Ge, Y.J.; Chen, Y.; Zhou, Y.Q.; Zhou, H.J. Experimental evidence of influential factor of quartz growth in reservoir. *J. China Univ. Pet.* **2010**, *34*, 13–18.
48. Yuanlin, M.; Cheng, X.; Hongyu, X.; Weizhi, T.; Chuanxin, T.; Jinghuan, L.; Youchun, W.A.; Yuting, G.A. A new kinetic model for authigenic quartz formation under overpressure. *Pet. Explor. Dev.* **2013**, *40*, 701–707.